

Comparison of Machine Learning Regression Methods to Simulate NO₃ Flux in Soil Solution under Potato Crops

J. G. Fortin^{1*}, A. Morais¹, F. Anctil¹, L. E. Parent²

¹Department of Civil and Water Engineering, Université Laval, Québec, Canada

²Department of Soils and Agrifood Engineering, Université Laval, Québec, Canada

Email: *jerome.goulet-fortin.1@ulaval.ca

Received 21 December 2013; revised 21 January 2014; accepted 28 January 2014

Copyright © 2014 by authors and Scientific Research Publishing Inc.

This work is licensed under the Creative Commons Attribution International License (CC BY).

<http://creativecommons.org/licenses/by/4.0/>



Open Access

Abstract

Nitrate (NO₃) leaching is a major issue in sandy soils intensively cropped to potato. Modelling could test the effect of management practices on nitrate leaching, particularly with regard to optimal N application rates. The NO₃ concentration in the soil solution is well known for its local heterogeneity and hence represents a major challenge for modeling. The objective of this 2-year-study was to evaluate machine learning regression methods to simulate seasonal NO₃ concentration dynamics in suction lysimeters in potato plots receiving different N application rates. Four machine learning function approximation methods were compared: multiple linear regressions, multivariate adaptive regression splines, multiple-layer perceptrons, and least squares support vector machines. Input candidates were chosen for known relationships with NO₃ concentration. The best regression model was obtained with a 6-inputs least squares support vector machine combining cumulative rainfall, cumulative temperature, day of the year, N fertilisation rate, soil texture, and depth.

Keywords

Machine Learning Regression; Nitrate Leaching; Suction Lysimeter; Potato Cropping System

1. Introduction

Groundwater nitrate (NO₃) contamination is particularly common in sandy soils intensively cropped to potato or other high-N demanding crops. Estimates of the apparent recovery of N fertiliser in the potato plant in Quebec ranged between 29% - 70% in loamy sands [1] and 21% - 62% in sandy soils [2]. Modeling could test the effect

*Corresponding author.

of management practices on nitrate leaching, particularly with regard to optimal N application rates.

Process-based NO₃ models require local soil, climatic, and management data as input, which are generally not available unless model calibration is the main intent [3]. Alternative approaches using empirical relationships between N soil status and surrogate variables may therefore fill that gap. Machine learning is one of the most important and useful data mining tools that can reveal non-linear interactions and patterns among data sets.

The objective of this study was to compare machine learning regression methods to simulate the seasonal dynamics of daily NO₃ flux (*NF*) from surrogate input variables. Four methods were evaluated: multiple linear regression (MLR) used here as reference model, multivariate adaptive regression splines (MARS), multiple-layer perceptrons (MLP), and least squares support vector machines (LS-SVM). Input candidates were selected for their known relationships with *NF*: N fertilization rate (N_{fert}), cumulative rainfall ($\Sigma rain$), cumulative temperature ($\Sigma temp$), day of the year (DOY), percentage of clay (% Clay), and soil depth (depth). The NO₃ losses in kg NO₃·ha⁻¹ are generally computed as the integral of the curve relating concentration to cumulative water loss [4]. Only NO₃ concentration was considered in this study.

2. Material and Method

The meteorological data were obtained at a daily time-step from a nearby micro-meteorological station from planting to harvest. In most N and C models, the minimum climatic input data requirement for simulating soil biological activity includes precipitation, temperature, and information on potential (or open pan) evapotranspiration. Because soil organic matter mineralization into inorganic N forms shows reportedly little sensitivity to evapotranspiration [5], only cumulative temperature and cumulative precipitation were considered.

Soil NO₃ concentration data were collected from 4rainfedpotato (*Solanum tuberosum* L.) fields located at Groupe Gosselin FG Inc. near Pont Rouge, Québec, Canada (Lat. 46°45'N; Long. 71°42'W). Each site was divided into three large blocks submitted to the following N treatments at planting: 0, 90, 130, and 170 kg·N·ha⁻¹. Soils were sampled in the spring at each site to determine particle-size distribution using the hydrometer method [6]. Suction lysimeters (model 1900L24-B02M2, Soil Moisture Equipment Corp., Ca) were installed into soil at planting. There were 3 replications per treatment, for a total of 36 lysimeters. Extraction of soil water from suction lysimeters was performed about 7 - 8 times each year. The NO₃ concentration of the solution was determined by liquid chromatography using a Dionex ICS2000 equipped with a UV-detector (Dionex Corporation, Sunnyvale, Ca). For each treatment, the results of 3 replications were averaged prior to modeling.

2.1. The Regression Models

2.1.1. Multiple Linear Regression

Multiple linear regression (MLR) was used as a reference model because of its simplicity and wide usage. It relates p explanatory variables x to *NF* at each time step t by fitting a linear equation to the data [7]:

$$\frac{dNF}{dt} = \mathbf{X}b + \varepsilon \quad (1)$$

where dNF/dt is a $n \times 1$ column vector (n = number of sampling occasions), \mathbf{X} is a $n \times (p+1)$ matrix, b is a $(p+1) \times 1$ column vector (the intercept b_0 and the slopes b_p), and ε is a $n \times 1$ vector of residuals that follows a multivariate normal distribution with mean of 0 and covariance matrix of $\mathbf{I}\sigma^2$, where \mathbf{I} is the identity matrix. The regression coefficient $b_1(b_2)$ reflects the partial effect of $x_1(x_2)$ when $x_2(x_1)$ is held constant:

$$\frac{\partial NF}{\partial x_1} = b_1, \frac{\partial NF}{\partial x_2} = b_2, \dots, \frac{\partial NF}{\partial x_p} = b_p \quad (2)$$

2.1.2. Multivariate Adaptive Regression Splines

The multivariate adaptive regression splines (MARS) simulates *NF* seasonal dynamics with M basis functions as follows [8]:

$$\frac{dNF}{dt} = c_0 + \sum_{m=1}^M c_m B_m(x) \quad (3)$$

where c_0 is a constant, $B_m(x)$ is the m^{th} basis function and c_m is coefficient of the m^{th} basis functions. MARS builds a model in two stages as forward and backward passes [9] [10]. During the forward pass, the algorithm starts with a “no-knowledge” model (*i.e.* the average response values at each time-step). Afterwards, the algorithm adds basis functions in pairs to the model. At each step, it finds the pair of functions producing maximum reduction of the error term. The two functions in the pair are identical except that a different side of a mirrored hinge function is used for each function. The addition of basis functions continues until the change in residual error becomes sufficiently small or until a pre selected maximum number of basis functions set sis reached. To avoid over-fitting, the backward pass prunes the model. It removes basis functions one by one, deleting the least effective ones at each step until it finds the best sub-model.

In order to determine which basis functions should be included in the model and to secure model generalization capacity, MARS exploits a generalized cross validation (GCV) [11] [10]: the mean squared residual error divided by a penalty depending on model complexity. The GCV criterion is defined as follows [12]:

$$\text{GCV} = \frac{\frac{1}{N} \sum_{i=1}^n [NF_i - \widehat{NF}]^2}{(1 - C(M)/n)^2} \quad (4)$$

where $C(M)$ is a complexity penalty that increases with the number of basis functions in the model [9]:

$$C(M) = (M + 1)/dM \quad (5)$$

where M is the number of basis functions in Equation (3) and d is a penalty for each basis function included in the model. It can be also regarded as a smoothing parameter. During this study, all MARS models were built using the ARES lab toolbox ver.1.5.1 [13].

2.1.3. Multiple-Layer Perceptron

Multiple-layer perceptron networks (MLPs) are also considered. They consist in a single layer of hidden neurons and a single output neuron. The MLP function of NF must be optimized at each time step across the following linear combination of multivariate functions:

$$\frac{dNF}{dt} = G_2 \left(\sum_j \left[\omega_j G_1 \left(\sum_{ij} \omega_{ij} x_i + \beta_j \right) + \beta \right] \right) \quad (6)$$

where x is an i^{th} -dimensional input vector, j is number of hidden neurons, ω are neural weights, and β are neural biases. The sigmoid tangent activation function G_1 and the linear activation function G_2 were computed as follows [14]:

$$G_1(\xi) = \frac{2}{1 + \exp(-2\xi)} - 1 \quad (7)$$

$$G_2(\xi) = \xi \quad (8)$$

where ξ is the weighted sum of information from the previous layer of neurons.

Stacking [15] was selected to support MLP’s generalization. This method calibrates several networks of the same architecture and simulates NF by calculating the mean of the responses across networks.

2.1.4. Least Squares Support Vector Machine

In SVM regression, the inputs are mapped in an m -dimensional feature space using some fixed (nonlinear) mapping, and a linear model is built in this feature space. Mathematically, it is given by [11]:

$$\frac{dNF}{dt} = \sum_{j=1}^m \omega \varphi(x) + \beta \quad (9)$$

where X is the input vector, ω the SVM weights vector, φ denotes a set of nonlinear transformations, and β is the bias. The algorithm performs regression in the high-dimension feature space using the ε -insensitive loss as cost function (see [11], for details) and, simultaneously, reduces model complexity minimizing $\|\omega\|^2$. This can be described by introducing the non-negative slack variables ξ_i and ξ_i^* that measure the deviation of the n training

samples outside the ε -insensitive zone (also named ε -tube). The SVM regression is thus formulated as a minimization of the following functional:

$$\text{Minimize } \rightarrow \frac{1}{2} \|\omega\|^2 + C \sum_{i=1}^n (\xi_i + \xi_i^*) \tag{10}$$

$$\text{Subject to } \left\{ \begin{array}{l} NF_i - \widehat{NF}_i - \beta \leq \varepsilon + \xi_i \\ \widehat{NF}_i + \beta - NF_i \leq \varepsilon + \xi_i^* \\ \xi_i, \xi_i^* \geq 0 \end{array} \right. \tag{11}$$

where the constant $C > 0$ determines the trade-off between the complexity of the model (flatness) and up to what deviations larger than ε are tolerated. Equation (11) implies that only data outside the ε -tube (*i.e.* “support vectors”) will be used in model building. This optimization problem can be transformed into a dual problem (see [16], for details) and its solution is given by:

$$\frac{dNF}{dt} = \sum_{i=1}^{n_{sv}} (a_i - a_i^*) K(\mathbf{x}_i, \mathbf{x}) \quad 0 \leq a_i^* \leq C, 0 \leq a_i \leq C \tag{12}$$

where n_{sv} is the number of support vectors, a_i, a_i^* are Lagrange multipliers, and K is a specified kernel function that measures the non-linear dependence between two instances of the input variables. Examples of kernel functions commonly used by SVMs are polynomial, radial basis, and sigmoid.

Least squares support vector machine (LS-SVM) is a reformulation of SVM. The LS-SVM uses a least squares loss function instead of the ε -insensitive loss function. It is known to be easier to optimize with shorter computational time [17]. In LS-SVM, the ε -tube and slack variables are replaced by error variables, which inform on the distances from each point to the regression function. All samples in LS-SVM are therefore support vectors, *i.e.* all training data are used to build the model. The regularization constant C (which was related to the ε -tube) is replaced by γ , determining the trade-off between the fitting error minimization and smoothness of the estimated function. Although the choice of kernel functions is the same as SVM, LS-SVM generally uses the radial basis function, which is defined as follow:

$$K(x, x_i) = \exp\left(-\|x - x_i\|^2 / 2\sigma^2\right) \tag{13}$$

where σ is a width parameter. The γ and σ parameters have to be determined by the user. All LS-SVM regression models were performed using the LS-SVM lab toolbox [18].

2.2. Model Calibration

The available 14 field plots were split into training and validation datasets; 65% of them were selected to train the model while the remaining was used for validation. To ensure statistical homogeneity between the training and testing datasets, a (1-d) Kohonen self-organizing feature map (KSFOM) [19] was constructed with maximal seasonal NF’s as input.

Input variables selection is a typical problem for machine learning. As the *a priori* knowledge of the problem led us considering few entries, a sequential forward selection was chosen for its simplicity. In sequential forward selection, the model inputs are first tested individually. Thereafter, following a stepwise method, combinations with an increasing number of variables are tested. The process stops when the addition of further variable stops increasing model’s performance. A first sequential forward selection was operated with a given set of model parameters. Once the best combination of variable was found, these parameters were optimized and a second sequential forward selection was done to ascertain that the best combination of variable did not change with the new parameter values. Only the performance obtained with the optimized parameters are presented here.

2.3. Evaluation

Model performance was evaluated calculating the Mean Absolute Error (MAE) and the Root Mean Square Error (RMSE) on NF —see [20] for details about these linear scoring rules.

The scale dependency of the linear scoring rules can be overcome using a skill score: a simple score standardization method that compares the performance of the simulation with that of a reference simulation. The Nash-

Sutcliffe efficiency index (NS) was used for this purpose [21]. A NS of 1 represents a perfect fit between simulated and observed values, while a NS of 0 is equivalent to a “no-knowledge” model, namely the mean of observations at every time step. Since scoring rules are averaged across the dataset, scatter plots are also drawn and regression lines are computed to visually assess the concordance and bias between simulated and observed *NF*.

3. Results and Discussion

Figure 1 presents the measured seasonal *NF* for all plots for the 2 seasons of the study. Because some of the lysimeters did not retain their tension in 2012, the 0 and 90 kg·N·ha⁻¹ treatments were only represented for one of the 2 sites in the first year. Note that all lysimeters did not collect water at every sampling time, explaining the disparities between time-series. The seasonal dynamics is generally characterized by a *NF* peak following N application at planting. As plants grew and took up nitrates, *NF* generally decreased as reported in previous studies (e.g. [22]). Averaged *NF* of the 32 operational lysimeters over the entire season of measure was 145 mg NO₃·L⁻¹, which is comparable to reported *NF* for sandy soil under potato in Quebec [23] [24]. A loose relationship between N treatment and *NF* can be observed at **Figure 1** (coefficient of correlation = 0.33). Higher maximal seasonal *NF*s were obtained with treatments of 130 and 170 kg·N·ha⁻¹ and the 0 treatment generally show low *NF* values. However, this relationship was not linear. For instance, one of the 170 kg·N·ha⁻¹ treatment in 2013 presented very low maximal *NF* while a 0 treatment presented relatively high *NF* in 2012 possibly due to stimulated and impaired growth patterns, respectively. This suggests that other explicative variables are required to reliably assess *NF*.

3.1. Modelling of NO₃ Flux Concentration

Statistics on models’ performance in training are presented in **Table 1**, while **Table 2** presents statistics on selected model performance for validation. The best MLR model was retained as reference (for brevity, only the best MLR is presented in **Table 2**). It contains input variable candidates, namely $\Sigma rain$, DOY, $\Sigma temp$, N_{fert} , depth and %clay. The NS reached 0.33 in training, with MAE of 79.2 mg NO₃ L⁻¹ (50.0% of the mean *NF* value of the calibration samples). Performance on testing, however, revealed complete absence of generalisation capacity of the linear approach. **Figure 2(a)** presents the scatter plot of observed and simulated *NF* using the best MLR during training and validation. Bias was close to 3000 mg NO₃ L⁻¹ during validation.

3.1.1. Multivariate Adaptive Regression Splines

For MARS, the variable explaining most variance was $\Sigma rain$ (NS = 0.24 in training), suggesting the importance of seasonal rainfall on NO₃ leaching. The DOY and $\Sigma temp$ also appeared influential with NS of about 0.2 in training. Depth and % clay did not weighted much at this step of the calibration. A 2-inputs MARS combining DOY and $\Sigma rain$ increased NS to 0.34 in training. The addition of $\Sigma temp$ and N_{fert} further increased performance, as suggested by the relationship between *NFC* and N_{fert} in **Figure 1**. The NS was 0.54 in training and the model

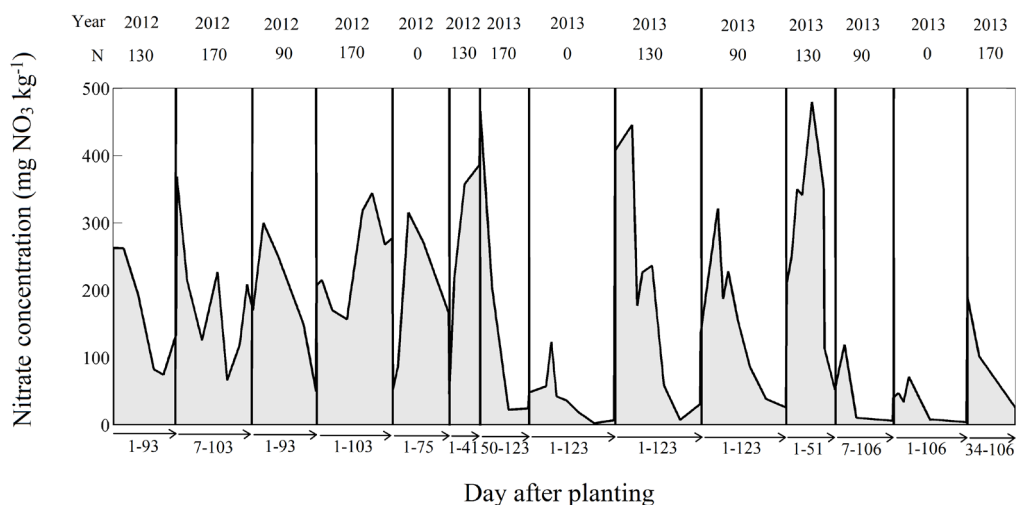


Figure 1. Seasonal dynamic of the measured NO₃ concentration (mg NO₃·L⁻¹).

Table 1. Statistics of model performance during training.

	RMSE	MAE	NS	r^2
	mg NO ₃ ·kg ⁻¹	mg NO ₃ ·kg ⁻¹		
MLR				
<i>Nfert</i> + DOY + Σ rain + Σ temp + depth + %Clay	101.21	79.25	0.33	Reference
MARS				
<i>Nfert</i>	110.64	88.63	0.20	-0.19
DOY	110.68	88.01	0.20	-0.20
Σ rain	107.76	79.56	0.24	-0.13
Σ temp	108.87	86.35	0.22	-0.16
% Clay	123.61	101.64	0.00	-0.49
Depth	120.77	92.89	0.04	-0.42
Σ rain + DOY	100.39	75.98	0.34	0.02
Σ rain + DOY + Σ temp	102.14	76.37	0.32	-0.02
Σ rain + DOY + Σ temp + <i>Nfert</i>	83.89	60.91	0.54	0.31
Σ rain + DOY + Σ temp + <i>Nfert</i> + depth	83.89	60.91	0.54	0.31
Σ rain + DOY + Σ temp + <i>Nfert</i> + %Clay	83.89	60.91	0.54	0.31
Σ rain + DOY + Σ temp + <i>Nfert</i> + %Clay + depth	83.89	60.91	0.54	0.31
MLP				
<i>Nfert</i>	110.64	88.63	0.20	-0.19
DOY	110.74	87.71	0.20	-0.20
Σ rain	107.64	80.11	0.24	-0.13
Σ temp	108.75	85.66	0.22	-0.15
% Clay	123.98	101.91	-0.01	-0.50
Depth	120.77	92.89	0.04	-0.42
Σ rain + DOY	103.61	76.98	0.30	-0.05
Σ rain + DOY + Σ temp	100.03	74.37	0.34	0.02
Σ rain + DOY + Σ temp + <i>Nfert</i>	66.30	46.75	0.71	0.57
Σ rain + DOY + Σ temp + <i>Nfert</i> + depth	64.00	44.55	0.73	0.60
Σ rain + DOY + Σ temp + <i>Nfert</i> + %Clay	59.59	43.35	0.77	0.65
Σ rain + DOY + Σ temp + <i>Nfert</i> + %Clay + depth	58.10	41.62	0.78	0.67
LS-SVM				
<i>Nfert</i>	110.64	88.63	0.20	-0.19
DOY	110.42	87.57	0.20	-0.19
Σ rain	109.98	81.13	0.21	-0.18
Σ temp	109.86	87.57	0.21	-0.18
% Clay	120.77	92.89	0.04	-0.42
Depth	105.47	82.58	0.13	-0.30
Σ rain + DOY	100.76	74.59	0.33	0.01
Σ rain + DOY + Σ temp	98.13	73.36	0.37	0.06
Σ rain + DOY + Σ temp + <i>Nfert</i>	43.94	28.43	0.87	0.81
Σ rain + DOY + Σ temp + <i>Nfert</i> + depth	43.73	28.28	0.87	0.81
Σ rain + DOY + Σ temp + <i>Nfert</i> + %Clay	21.77	15.89	0.97	0.95
Σ rain + DOY + Σ temp + <i>Nfert</i> + %Clay + depth	21.70	15.93	0.97	0.95

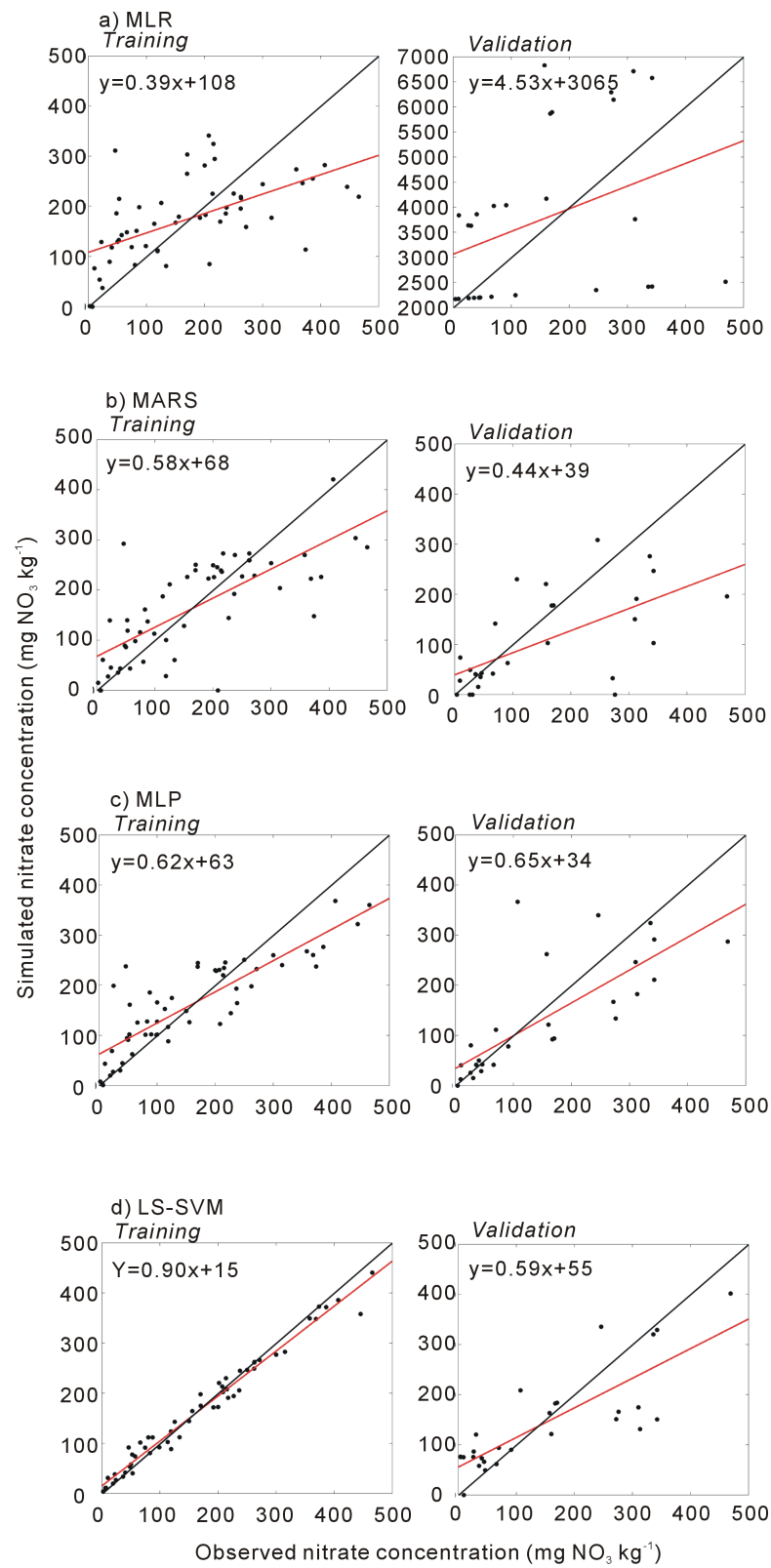


Figure 2. Scatter plot of the measured and simulated NO₃ concentration (mg·NO₃·L⁻¹). The black line indicates the 1:1 line (perfect fit).

Table 2. Statistics of the selected model performance during validation.

	RMSE	MAE	NS	r^2
	mg NO ₃ ·kg ⁻¹	mg NO ₃ ·kg ⁻¹		
MLR				
$Nfert + DOY + \Sigma rain + \Sigma temp + depth + \% Clay$	3936.10	3590.50	-873	Reference
MARS				
$\Sigma rain + DOY + \Sigma temp + Nfert$	113.27	76.00	0.28	1.00
MLP				
$\Sigma rain + DOY + \Sigma temp + Nfert + \% Clay$	92.03	64.07	0.52	1.00
LS-SVM				
$\Sigma rain + DOY + \Sigma temp + Nfert + \% Clay + depth$	78.30	58.16	0.65	1.00

was able to explain about 30% more variance than the reference model ($r^2 = 0.3$). Further addition of depth and % clay did not improve model's performance. Even though the generalisation capacity was highly improved as compared to MLR, it remained low with NS of 0.28 in validation. **Figure 2(b)** presents the scatter plot of observed and simulated NF using the best 4-inputs MARS. Compared to the reference model, the regression lines were closer to 1:1 and the intercept closer to 0, but scattering remained high especially in validation. The optimal maximal number of basis functions was 11.

3.1.2. Multiple-Layer Perceptron

Performances of the 1 to 3 inputs MLPs were similar to those of the MARS models. The main difference between these approaches was that the addition of depth and % clay substantially increased MLP performance. A 5-inputs MLP combining $\Sigma rain$, DOY, $\Sigma rain$, $Nfert$ and % clay yielded NS of 0.77 in training. The generalisation capacity of the model appeared relatively good compared to the reference model, with NS of 0.52. The gain in performance over the linear model was substantial ($r^2 = 0.65$). The scatter plot of the best 5-inputs MLP (**Figure 2(c)**) showed better fit than the best MARS, particularly in validation. The optimal number of hidden nodes was 3.

3.1.3. Least Squares Support Vector Machine

The optimal values for LS-SVM parameters γ and σ were 11 and 1.1, respectively, compared to default values of 10 and 0.3 suggested in the LS-SVM lab toolbox. This larger σ indicates that more relative weights were given to points with larger distance from the regression function.

The 1 to 3 inputs LS-SVMs performed similarly as MARS and MLP. However, compared to MLP, the LS-SVMs showed higher sensitivity to depth and % clay. In training, NS of the best 6-input models (combining all input candidates) reached 0.95, with MAE as low as 15.9 mg NO₃ kg⁻¹ (10% of the mean NF value of the training dataset). Mean bias appeared significantly smaller than what was obtained in a previous study on potato fields within the same geographical location using transfer functions [24]. As expected, performance considerably decreased in validation, but less than the previous methods. The NS was 0.65 and MAE was 58.2 mg NO₃ kg⁻¹ (46% of the mean NF value of the validation dataset). **Figure 2(d)** revealed the very close fit of the 6-inputs LS-SVM in training. In calibration, however, the bias was higher than MLP, even though the scattering was slightly narrower.

These results suggests that the proposed 6-inputs LS-SVM performed best for general diagnostic of N leaching risk considering soil texture, local meteorological condition and N fertilisation rates. Further inclusion of spatial surrogate variables at field level (ex: leaf area index) could contribute reducing the error even more. **Figure 3** presents the architecture of the final LS-SVM model and its general expression.

4. Conclusion

This study highlighted the non-linearity of NO₃ flux in the soil solution and the need to rely on non-linear regression methods for its characterization. The best regression model was obtained with a 6-input least squares support vector machine combining cumulative rainfall, cumulative temperature, day of the year, N fertilisation

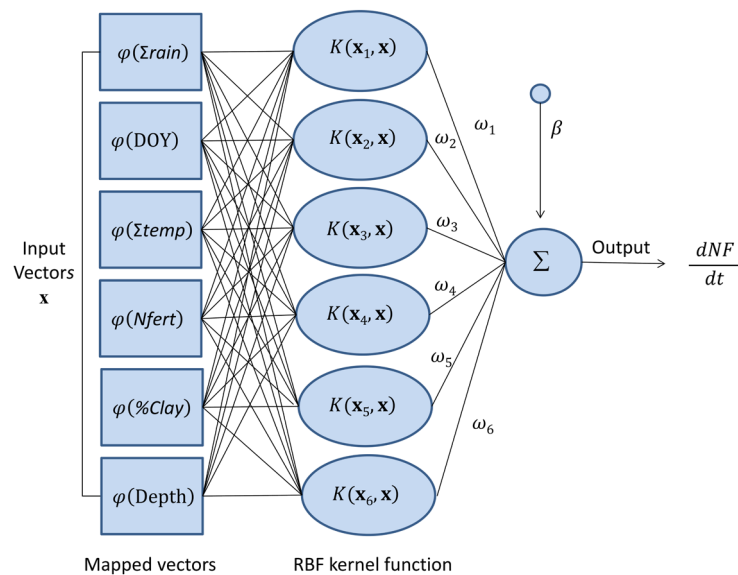


Figure 3. Architecture of the final 6-input LS-SVM and its general expression.

rate, soil texture, and depth. Performance in validation is satisfying considering the challenge that represents the NO_3 flux concentration modeling of the soil solution. Further addition of spatial surrogate variables such as the leaf area index could improve the generalisation capacity of the model.

Acknowledgements

This project was funded by the Natural Sciences and Engineering Council of Canada (CRDPJ 385199-09) and the following cooperative partners: Cultures Dolbec Inc. (St-Ubalde, Québec), Groupe Gosselin FG Inc. (Pont Rouge, Québec), Agriparmentier Inc. (Notre-Dame-du-Bon-Conseil, Québec), and Ferme Daniel Bolduc et Fils Inc. (Péribonka, Québec).

References

- [1] Li, H., Parent, L.-E., Karam, A. and Tremblay, C. (2003) Efficiency of Soil and Fertilizer Nitrogen of a Sod-Potato System in the Humid, Acid and Cool Environment. *Plant and Soil*, **251**, 23-26. <http://dx.doi.org/10.1023/A:1022983830986>
- [2] Cambouris, A.N., Zebarth, B.J., Nolin, M.C. and Laverdière, M.R. (2008) Apparent Fertilizer Nitrogen Recovery and Residual Soil Nitrate under Continuous Potato Cropping: Effect of N Fertilization Rate and Timing. *Canadian Journal of Soil Science*, **88**, 813-825. <http://dx.doi.org/10.4141/CJSS07107>
- [3] Jiang, Y., Zebarth, B.J., Somers, G.H., MacLeod, J.A. and Savard, M.M. (2012) Nitrate Leaching from Potato Production in Eastern Canada. In: He, Z., Larkin, R.P. and Honeycutt, C.W., Eds., *Sustainable Potato Production: Global Case Studies*, Springer, The Netherlands, 233-250. http://dx.doi.org/10.1007/978-94-007-4104-1_13
- [4] Lord, E.I. and Shepherd, M.A. (1993) Development in the Use of Porous Ceramic Cum for Measuring Nitrate Leaching. *Journal of Soil Science*, **44**, 435-449. <http://dx.doi.org/10.1111/j.1365-2389.1993.tb00466.x>
- [5] Fortin, J.G., Bolinder, M.A., Anctil, F., Kätterer, T., André, O. and Parent, L.-E. (2011) Effects of Climatic Data Low-Pass Filtering on the ICBM Temperature- and Moisture-Based Soil Biological Activity Factors in a Cool and Humid Climate. *Ecological Modelling*, **222**, 3050-3060. <http://dx.doi.org/10.1016/j.ecolmodel.2011.06.011>
- [6] Sheldrick, B.H. and Wang, C. (1993) Particle Size Analysis. In: Carter, M.R., Ed., *Soil Sampling and Methods of Analysis*, Lewis Publishers, Boca Raton, 499-517.
- [7] Rosner, B. (2006) *Fundamentals of Biostatistics*. Duxbury Press, Boston, 6th Edition.
- [8] Friedman, J.H. and Roosen, C.B. (1995) An Introduction to Multivariate Adaptive Regression Splines. *Statistical Methods in Medical Research*, **4**, 197-217. <http://dx.doi.org/10.1177/096228029500400303>
- [9] Friedman, J.H. (1991) Multivariate Adaptive Regression Splines. *Annals of Statistics*, **19**, 1-141. <http://dx.doi.org/10.1214/aos/1176347963>

- [10] García Nieto, P.J., Martínez Torres, J., de Cos Juez, F.J. and Sánchez Lasheras, F. (2012) Using Multivariate Adaptive Regression Splines and Multilayer Perceptron Networks to Evaluate Paper Manufactured Using *Eucalyptus globulus*. *Applied Mathematics and Computation*, **219**, 755-763. <http://dx.doi.org/10.1016/j.amc.2012.07.001>
- [11] Vapnik, V. (1998) *Statistical Learning Theory*. Wiley-Interscience, New York.
- [12] Chou, S.M., Lee, T.S., Shao, Y.E. and Chen, I.F. (2004) Mining the Breast Cancer Pattern Using Artificial Neural Networks and Multivariate Adaptive Regression Splines. *Expert Systems with Applications*, **27**, 133-142. <http://dx.doi.org/10.1016/j.eswa.2003.12.013>
- [13] Jekabsons, G. (2013) ARESLab: Adaptive Regression Splines Toolbox for Matlab/Octave. <http://www.cs.rtu.lv/jekabsons/>
- [14] Yonaba, H., Anctil, F. and Fortin, V. (2010) Comparing Sigmoid Transfer Functions for Neural Network Multistep Ahead Streamflow Forecasting. *Journal of Hydrologic Engineering*, **15**, 275-283. [http://dx.doi.org/10.1061/\(ASCE\)HE.1943-5584.0000188](http://dx.doi.org/10.1061/(ASCE)HE.1943-5584.0000188)
- [15] Wolpert, D.H. (1992) Stacked Generalisation. *Neural Network*, **5**, 241-259. [http://dx.doi.org/10.1016/S0893-6080\(05\)80023-1](http://dx.doi.org/10.1016/S0893-6080(05)80023-1)
- [16] Asefa, T., Kemblowski, M.W., Urroz, G., McKee, M. and Khalil, A. (2004) Support Vectors-Based Groundwater Head Observation Networks Design. *Water Resources Research*, **40**, W11509. <http://dx.doi.org/10.1029/2004WR003304>
- [17] Wang, W.J., Xu, Z.B., Lu, W.Z. and Zhang, X.Y. (2003) Determination of the Spread Parameter in the Gaussian Kernel for Classification and Regression. *Neurocomputing*, **55**, 643-663. [http://dx.doi.org/10.1016/S0925-2312\(02\)00632-X](http://dx.doi.org/10.1016/S0925-2312(02)00632-X)
- [18] Pelckmans, K., Suykens, J.A.K., Van Gestel, T., De Brabranter, J., Lukas, L., Hamers, B., De Moor, B. and Vandewalle, J. (2003) LS-SVMLab Toolbox User's Guide, Version 1.5. ESAT-SCD-SISTA Technical Report 02-14. <http://www.esat.kuleuven.ac.be/sista/lssvmlab/>
- [19] Kohonen, T. (1982) Self-Organized Formation of Topologically Correct Feature Maps. *Biological Cybernetics*, **43**, 59-69. <http://dx.doi.org/10.1007/BF00337288>
- [20] Fortin, J.G., Bolinder, M.A., Anctil, F., Kätterer, T., Andrén, O. and Parent, L.E. (2011) Effects of Climatic Data Low-Pass Filtering on the ICBM Temperature- and Moisture-Based Soil Biological Activity Factors in a Cool and Humid Climate. *Ecological Modelling*, **222**, 3050-3060. <http://dx.doi.org/10.1016/j.ecolmodel.2011.06.011>
- [21] Nash, J.E. and Sutcliffe, J.V. (1970) River Flow Forecasting through Conceptual Models: A Discussion of Principles. *Journal of Hydrology*, **10**, 282-290. [http://dx.doi.org/10.1016/0022-1694\(70\)90255-6](http://dx.doi.org/10.1016/0022-1694(70)90255-6)
- [22] Sharifi, M., Zebarth, B.J., Hajabbasi, M.A. and Kalbasi, M. (2005) Dry Matter and Nitrogen Accumulation and Root Morphological Characteristics of Two Clonal Selections of "Russet Norkotah" Potato as Affected by Nitrogen Fertilization. *Journal of Plant Nutrition*, **28**, 2243-2253. <http://dx.doi.org/10.1080/01904160500323552>
- [23] Gasser, M.O. (2000) Transformation et Transfert de L'azote dans les Sols Sableux Cultivés en Pomme de Terre. Ph.D. Thesis, Université Laval, Ste-Foy.
- [24] Gasser, M.O., Caron, J., Lagacé, R. and Laverdière, M.R. (2003) Predicting Nitrate Leaching under Potato Crops Using Transfer Functions. *Journal of Environmental Quality*, **32**, 1464-1473. <http://dx.doi.org/10.2134/jeq2003.1464>